New allotropes of phosphorene with remarkable stability and intrinsic piezoelectricity

Zhenqing Li,[1,2] Chaoyu He,[1,2,*] Tao Ouyang,[1,2] Chunxiao Zhang,[1,2]
Chao Tang,[1,2,†] Rudolf A. Röemer,[3,2,‡] and Jianxin Zhong[1,2,§]

[1]*Hunan Key Laboratory for Micro-Nano Energy Materials and Devices, Xiangtan University, Hunan 411105, P. R. China;*
[2]*School of Physics and Optoelectronics, Xiangtan University, Xiangtan 411105, China.*
[3]*Department of Physics, University of Warwick, Coventry, CV4 8UW, UK.*

(Dated: March 17, 2018)

We construct a new class of two-dimensional (2D) phosphorus allotropes via assembling the previously proposed ultrathin metastable phosphorus nanotube into planar structures in different stacking orientations. Based on first-principle methods, the structures, stabilities and fundamental electronic properties of these new 2D phosphorus allotropes are systematically investigated. Our results show that these 2D van der Waals phosphorene allotropes possess remarkable stabilities due to the strong inter-tube van der Waals interactions, which cause an energy release of about 30-70 m*e*V/atom depending on their stacking details. Most of them are confirmed energetically more favorable than the experimentally viable α-P and β-P. Three of them, showing relatively higher probability to be synthesized in the future, are further confirmed to be dynamically stable semiconductors with strain-tunable band gaps and intrinsic piezoelectricity, which may have potential applications in nano-sized sensors, piezotronics, and energy harvesting in portable electronic nano-devices.

PACS numbers: 73.20.At, 61.46.-w, 73.22.-f, 73.61.Cw

INTRODUCTION

The experimental discovery of piezoelectricity in two-dimensional (2D) materials, such as the hexagonal MoS_2 [1–3] and carbon nitride (C3N4) [4], leads nano-scale piezoelectricity becomes a very hot topic in recent years [5–8]. Large numbers of 2D material have been reported as potential piezoelectric materials with remarkable piezoelectric coefficients comparable to traditional three-dimensional (3D) piezoelectric materials. For example, the metal dichalcogenides (MX_2, M=Cr, Mo, W, Nb, Ta; X=S, Se, Te) [3, 7, 9–13], the hexagonal group III-V (MX, M=B, Al, Ga, In, X=N, P, As, Sb) [7, 12, 14, 15], the group II oxides [7, 16], and the group-IV monochalcogenides (GeS, GeSe, SnS and SnSe) [5, 6, 17–20]. These new discoveries significantly expanded the application fields of these 2D materials to nano-sized sensors, piezotronics and energy harvesting in portable electronic nano-devices[21, 22].

Black phosphorene (α-P) [23, 24] is a new 2D materials experimentally synthesized in the same year of the experimental discovery of 2D piezoelectricity [1]. It is considered as a formidable competitor to graphene and other two-dimensional (2D) materials for applications in future nano-electronics due to its significant band gap [25, 26] and high carrier mobility [23, 25]. Blue phosphorene (β-P), another 2D phosphorus allotrope, was firstly proposed by Zhu et al. based on first-principles calculations [27] in 2014 and recently synthesized by Zhang et al. through epitaxial growth method [28]. The progress in synthesis of 2D phosphorus materials [29–31] has stimulated significant interests in exploring new 2D phosphorus materials [32–41] and related heterostructures [42–44]. Many new 2D allotropes of phosphorus have been proposed. For example, the atomically-thin layers of γ-P [32], δ-P [32], θ_0-P [33] and red phosphorene [34], the diatomically-thin layers η-P [35], θ-P [35] and their transformations [36] (G1, G2, B1, B2 and B3) with pentagons, the multi-atomically-thin layer of Hittorfene [37], as well as the porous phosphorene allotropes were previously proposed [38, 39] through the topological modeling method. However, none of these 2D phosphorus allotropes were reported as piezoelectric materials due to their centrosymmetric crystalline structures. Recently, a non-centrosymmetric one-dimensional phosphorus nanotube was theoretically predicted [40], which is expected to be potential piezoelectric material. Very interesting, its corresponding allotropes (*helical coil* phosphorus) have been experimentally synthesized [41] in a carbon nanotube reactor.

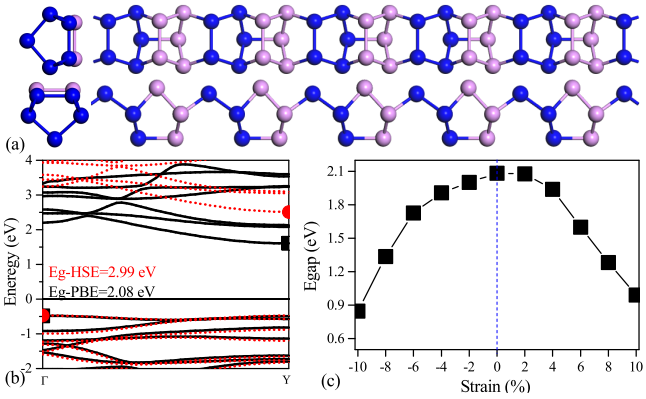

FIG. 1. Schematic crystalline views of um-PNT from different directions (a), where blue balls and purpule balls illustrate the pentagonal configurations of phosphorus atoms in two different arrangements, the calculated electron band structures of um-PNT (b), where the black solid lines are calculated from normal density functional theory and the red dash lines are calculated from hybrid functional method (HSE06), and the strain dependence of band gaps in um-PNT (c).

Phosphorene allotropes with lone pairs on the surface similar to SnS and SnSe [5, 6] are expected to be excellent 2D piezoelectric materials[1, 2, 7, 12, 45]. However, the exper-

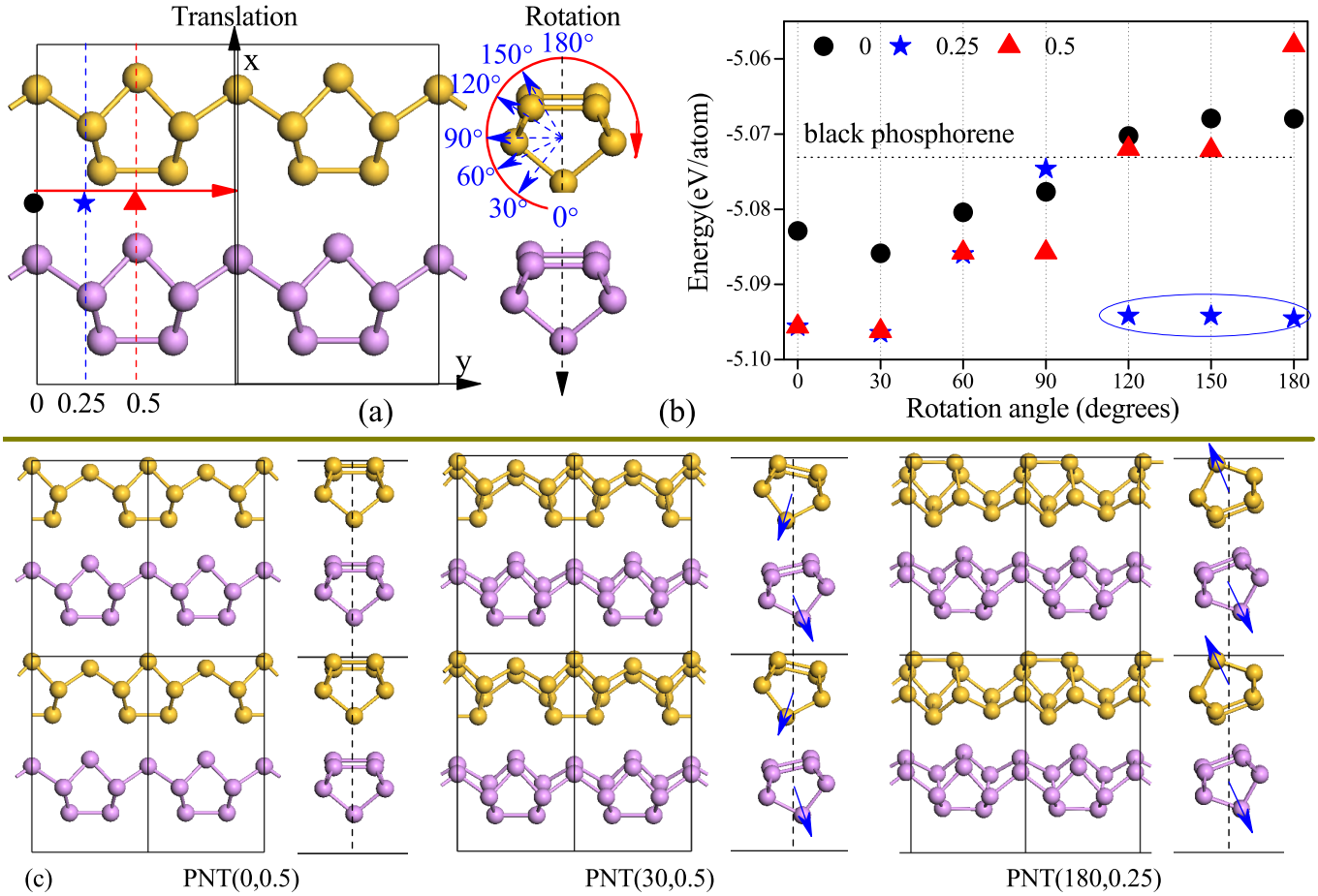

FIG. 2. Sketch map of the translation and self-rotation for assembling 1D um-PNT (the atoms of the yellow one are free to adjust their positions and the atoms positions of the purple one are fixed in its initial operation, but all atoms are free to move in the process of optimization.) into 2D phosphorus allotropes PNT(θ, τ) (a). The calculated average energy for the 21 new 2D van der Waals phosphorene allotropes PNT(θ, τ) with different rotation angle θ and translation τ, where black circles, blue stars, and red triangles correspond to $\tau = 0, 0.25$, and 0.5, respectively (b). The crystalline views of the most stable three ones, PNT(0,0.5), PNT(30,0.5) and PNT(180,0.25) (c).

imentally viable α-P and β-P, as well as most of the previously proposed 2D allotropes of phosphorus, are centrosymmetric and consequently non-polar, which indicates that they are non-piezoelectric. Inspired by the discovery of the non-centrosymmetric phosphorus nanotube and its synthesizing, we theoretically predicted a new class of 2D van der Waals crystals of phosphorus via planer stacking of the previously proposed ultrathin metastable phosphorus nanotube (um-PNT, P_∞[40]). Three of them are confirmed to be dynamically stable allotropes and energetically more favorable than the experimentally viable α-P and β-P. Especially, two of them with non-centrosymmetric stacking manners are confirmed to be good piezoelectric materials, which have potential applications in nano-sized sensors, piezotronics, and energy harvesting in portable electronic nano-devices.

METHODS

Our calculations were carried out by using the density functional theory (DFT) within generalized gradient approximations (GGA)[46] as implemented in the Vienna ab initio simulation package (VASP)[47, 48]. The interactions between nucleus and the $3s^2 3p^3$ valence electrons of phosphorus atoms were described by the projector augmented wave (PAW) method[49, 50]. A plane-wave basis with a cutoff energy of 500 eV was used to expand the wave functions. The Brillouin zone integration was obtained by a $5 \times 8 \times 1$ k-point grid. We have used the Monkhorst-Pack k-mesh scheme with $7 \times 11 \times 1$ to check the accuracy and found the same results. The structures of all phosphorene allotropes were fully optimized up to the residual force on every atom less than 0.001 eV/Å before investigating any material properties.

The optimized exchange van der Waals functional (optB86b-vdW) [51, 52] was also applied to take into account van der Waals interactions in the systems. We know that there

have some debates about the vdW [53, 54]. However, our testing tasks show that the order of energetic stability for these phosphorene allotropes are not changed in different functionals. The vibrational properties of the three new phosphorene allotropes more favorable than α-P and β-P were investigated through the MEDEA-PHONON package [55] with the forces calculated from VASP to confirm their dynamical stabilities. In our calculations, the finite displacement method was used. Our calculations considered use normal DFT functional without vdW correction to calculate the vibrational spectrum of our new allotropes. The testing task shows that the results with vdW correction always leads little imaginary frequency around the Γ-point, which can be understood as calculational error but not structural instability.

RESULTS AND DISCUSSION

structures and stabilities

The crystal structure of the um-PNT [40] consists of phosphorus pentagons as shown in Fig. 1 (a). It is structurally very similar to the fundamental structure-units in violet phosphorus and red phosphorus [37, 56, 57]. Our calculated results show that it is of about 44 meV/atom higher in energy than the α-P. And it is more favorable than most of the previously proposed 2D phosphorene allotropes. In particular, um-PNT [40] is also more stable than most of the previously proposed a-PNTs and z-PNTs [32, 58]. The smallest phosphorus tube proposed before is the a-PNT with tube radius of about 2.3 Å, which is of about 100 meV/atom higher than black phosphorene and less stable than um-PNT [40]. The radius of um-PNT is only 1.6 Å, which indicates that um-PNT [40] is the smallest phosphorus tube so far. The DFT-based band structure shown in Fig. 1 (b) indicates that um-PNT is a semiconductor with indirect band gap of about 2.08 eV. Its HSE06-based band gap is of about 2.99 eV. Further DFT-based investigations show that um-PNT is a good candidate for 1D semiconductor applications in view of that its band gap can be effectively modulated by strains.

As shown in Fig. 2 (a), two um-PNTs are arranged in an orthorhombic cell as a starting structure, in which the violet tube is fixed and the yellow one is free for operation. Based on the well defined operators T_τ (translation, $\tau = 0, 0.25$ and 0.5 **b**) and R_θ (self-rotation, $\theta = 0°$, 30°, 60°, 90°, 120°, 150° and 180°) as indicated in Fig. 2 (a), 21 initial structures can be constructed. We denote them as PNT(θ, τ) according to the operation (R_θ,T_τ) applied on the free yellow tube, where θ means the rotation angle and τ denotes the translation vector. For example, PNT(180,0.25) indicates the mutation of the initial structure PNT(0,0) through a self-rotation of 180° and a translation of 0.25 **b** along the tube direction (y direction) on the yellow tube.

We then optimized the crystalline structures of these 21 new phosphorus allotropes through first-principles calculations. The calculated total energies of α-P and the 21 new

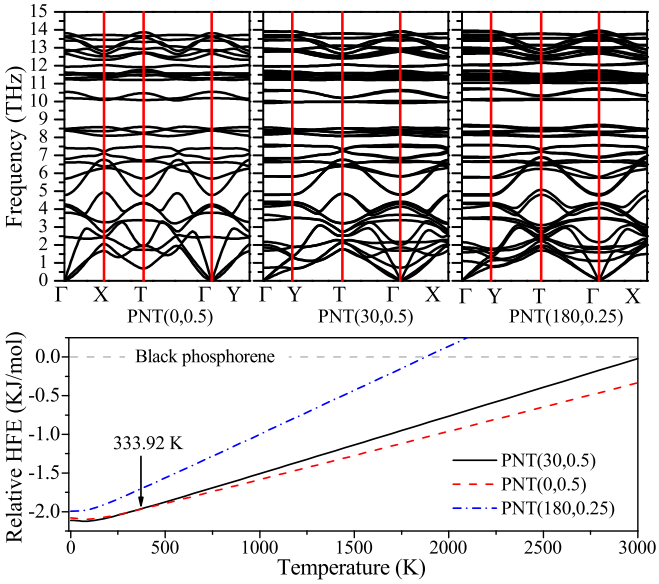

FIG. 3. The calculated *phonon* band structures (top) of PNT(0,0.5), PNT(30,0.5) and PNT(180,0.25) as well as their Helmholtz free energies (bottom) relative to that of α-P.

2D van der Waals phosphorus allotropes are shown in Fig. 2 (b). According to our results, all these new 2D phosphorus allotropes are more stable in energy than the 1D um-PNT by about 30-70 meV/atom, dependent on the assembling manner. With the remarkable release of energy after assembling into a planar array, most of the new 2D phosphorus allotropes are energetically more stable than α-P and β-P. From the results in Fig. 2 (b), we can see that some initial structures are degenerate in energy after optimization. We checked the optimized structures and found that PNT(0,0.25), PNT(30,0.25) and PNT(60,0.25) are degenerate to PNT(0,0.5), PNT(30,0.5) and PNT(60,0.5), respectively. Both PNT(120,0.25) and PNT(150,0.25) are degenerate to PNT(180,0.25). We further confirmed that the most stable three structures are PNT(0,0.5), PNT(30,0.5) and PNT(180,0.25), whose energies are of about 22 meV/atom, 23 meV/atom and 21 meV/atom lower than that of the black phosphorene. The crystal structures of these three most stable ones are shown in Fig. 2 (c), where we can see that they are obviously different from each other. We also found that PNT(0,0.5) keeps its initial structure well in the optimization process, but PNT(30,0.5) and PNT(180,0.25) have obvious changes in orientation angle as indicated in Fig. 2 (c).

From the view of thermodynamics, a structure with lower energy generally implies a higher probability to be synthesized in experiments if it is dynamically possible. PNT(0,0.5), PNT(30,0.5) and PNT(180,0.25) have remarkable stabilities exceeding α-P and are expected to be synthesized in the near future using, e.g., vapor deposition methods. The dynamical stabilities of the three new phosphorene allotropes thus need to be confirmed for the viability of their synthesis. We studied their vibrational properties through the PHONON package combined with VASP. The results are shown in Fig. 3. We find

that the phonon band structures of PNT(0,0.5), PNT(30,0.5) and PNT(180,0.25) are free of soft modes associated with structural instability. We also examined the whole BZ and found no imaginary states in their phonon density of states. The results show that allotropes PNT(0,0.5), PNT(30,0.5) and PNT(180,0.25) are dynamically viable.

Based on the calculated vibrational spectra, we then calculated the Helmholtz free energies and compared them with that of the α-P. As shown in Fig. 3, we can see that PNT(0,0.5), PNT(30,0.5) and PNT(180,0.25) are always energetically more favorable than α-P in the temperature range of 0-1700 K. PNT(0,0.5) and PNT(30,0.5) are always more stable than PNT(180,0.25) in the whole temperature range. Interestingly, PNT(30,0.5) is energetically more stable than PNT(0,0.5) below 333.29 K and it becomes less stable than PNT(0,0.5) when the temperature is higher than 333.29 K.

Electronic properties

The electronic band structures of allotropes PNT(0,0.5), PNT(30,0.5) and PNT(180,0.25) were investigated by first-principles calculations. As shown in Fig. 4 (a), we see that PNT(0,0.5), PNT(30,0.5) and PNT(180,0.25) are indirect band gap semiconductors with band gaps of 1.430 eV, 1.522 eV and 1.574 eV, respectively. The calculated effective masses of the electrons (holes) along the tube direction (Γ-Y direction) in PNT(0,0.5), PNT(30,0.5) and PNT(180,0.25) are 0.33 m_0 (0.999 m_0), 0.44 m_0 (0.95 m_0) and 0.54 m_0 (1.71 m_0), respectively. Effective masses of electrons and holes along the another direction cross the tube are not considered here. As discussed above, um-PNT is an indirect band gap semiconductor with a band gap of 2.08 eV, which is larger than those of PNT(0,0.5), PNT(30,0.5) and PNT(180,0.25). That is to say, the inter-tube van der Waals interactions reduce the band gap of the system after assembly. We notice that such a phenomenon is very similar to that of stacking single layers of α-P or β-P into multi-layer [25, 27, 59]. Accordingly, we can effectively modulate the electronic properties of these new 2D phosphorus allotropes by adjusting the inter-tube distance by strain [60].

Fig. 4 (b) are the band gaps of PNT(0,0.5), PNT(30,0.5) and PNT(180,0.25) under different strains. We can see that compressive (tensile) strains across the tube reduce (increase) the inter-tube distance and correspondingly reduce (increase) the band gap of the systems. These results are very similar to those in three-dimensional bulk black phosphorus, whose band gap can be effectively modulated by inter-layer distance. The modulating effects of strains along the tube on the band gaps of PNT(0,0.5), PNT(30,0.5) and PNT(180,0.25) are expected to be similar to that of um-PNT where both compressive and tensile strains reduce the band gaps (see in Fig. 1 (c)). However, the results in Fig. 4 (b) have some differences in comparison with Fig. 1 (c), especially in the compressive area. For example, in single um-PNT, the band gap always decreases as the compressive strain increases but the band gap

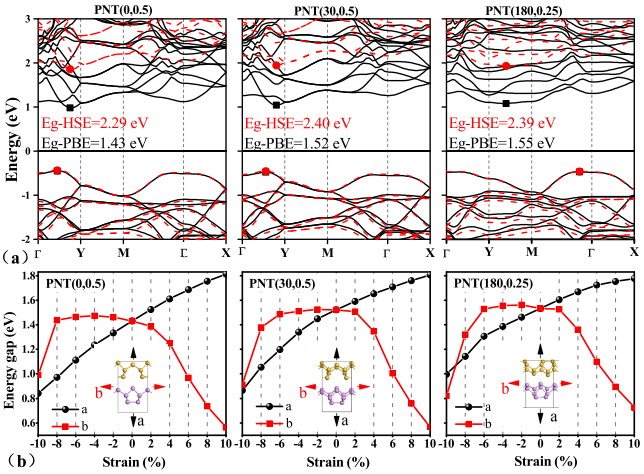

FIG. 4. The calculated *electron* band structures of PNT(0,0.5), PNT(30,0.5) and PNT(180,0.25) (a), where the black solid lines are calculated from normal density functional theory and the red dash lines are calculated from hybrid functional method (HSE06), and the corresponding modulating effects of stains on their band gaps as indicated by the schematics in each bottom panel (b).

of PNT(0,0.5) slightly increases at first under small compressive strain and then decreases under larger compressive strain. Such a phenomenon is due to the inter-tube van der Waals interaction in PNT(0,0.5), PNT(30,0.5) and PNT(180,0.25). The compressive strain along the tube first reduces the band gap of the tube itself. Eventually it will also increase the inter-tube distance and thus correspondingly increase the band gap of the system. Consequently, small compressive strain along the tube slightly increase the band gap of the system.

Piezoelectric properties

In our present work, we notice that PNT(0,0.5) and PNT(30,0.5) are allowed to be piezoelectric according to their non-centrosymmetric and polar space groups, *Amm*2 and *Pmn*21, respectively. Their puckered $C2v$ symmetries are very flexible along the direction perpendicular to the tube (x direction), which are expected to further enhance the piezoelectricity. Based on the widely used methodology [5–7, 12, 45] for quasi two-dimensional materials, the piezoelectric coefficients e^{2D}_{ijk} and d^{2D}_{ijk} of PNT(0,0.5) and PNT(30,0.5) are calculated as the third-rank tensors as the relative polarization vector P^{2D}_i to strain ε_{jk} and stress σ_{jk}, e.g.

$$e^{2D}_{ijk} = \frac{\partial P^{2D}_i}{\partial \varepsilon_{jk}}, \quad d^{2D}_{ijk} = \frac{\partial P^{2D}_i}{\partial \sigma_{jk}}. \tag{1}$$

With mirror symmetry along the tube direction (y direction), the independent piezoelectric coefficients for PNT(0,0.5) and PNT(30,0.5) are (e^{2D}_{111}, e^{2D}_{122}, $e^{2D}_{212} = e^{2D}_{221}$) and ($d^{2D}_{111}$, d^{2D}_{122}, $d^{2D}_{212} = d^{2D}_{221}$). Indices 1 and 2 correspond to the x and y

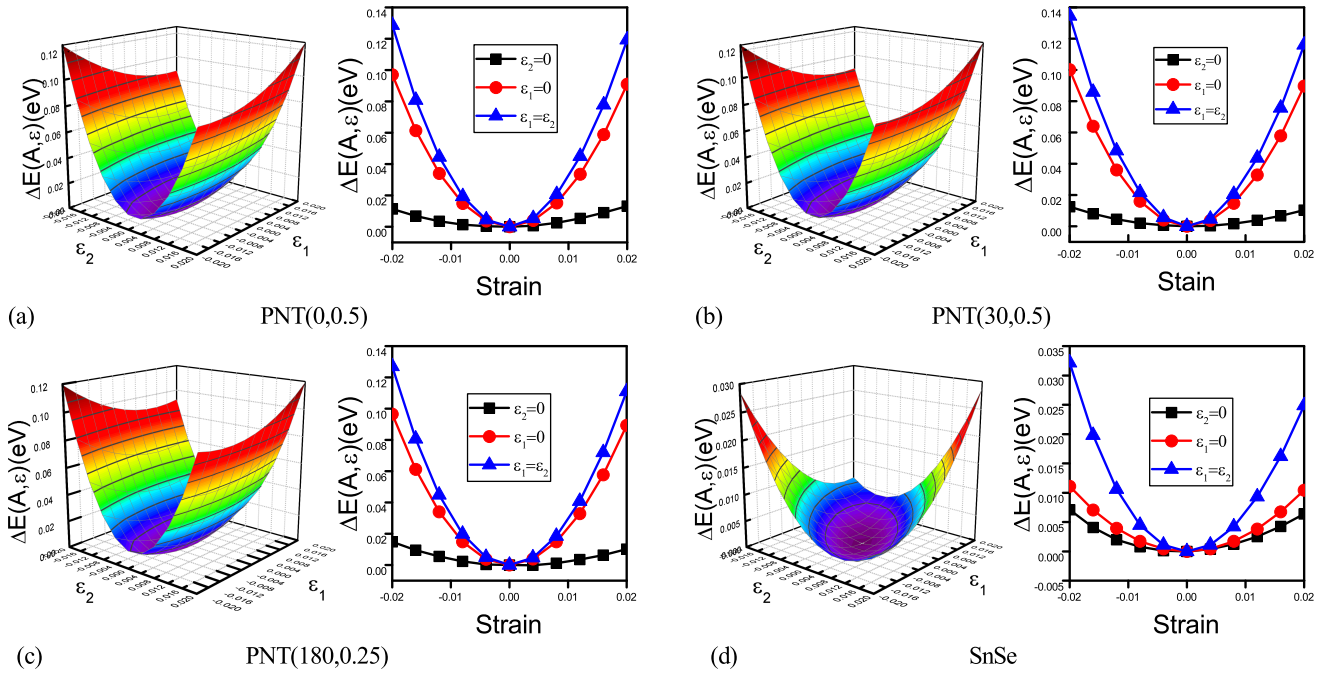

FIG. 5. The three-dimensional surface plot of the total energy(in eV) versus a series of strain states (ε_{11},ε_{22}) for PNT(0,0.5), PNT(30,0.5), PNT(180, 0.25) and SnSe, respectively.

directions as indicated in Fig. 2 (a). Here, we just consider the responses of polarization P_1^{2D} along x direction to strain (stress) ε_{11} (σ_{11}) and ε_{22} (σ_{22}) along x and y directions, respectively. Response of polarization P_1^{2D} to shear strain ε_{12} (stress σ_{12}) is not considered in our calculation. Polarization P_2^{2D} along the y direction is always zero due to the mirror symmetry. Using the Voigt notation [61], we simplify the coefficients as (e_{11}^{2D}=e_{111}^{2D}, e_{12}^{2D}=e_{122}^{2D}) and (d_{11}^{2D}=d_{111}^{2D}, d_{12}^{2D}=d_{122}^{2D}). The piezoelectric coefficients e_{11}^{2D} and e_{12}^{2D} for PNT(0,0.5) and PNT(30,0.5) are obtained by least-squares fitting of the polarization change per unit area to the following equation

$$P_1^{2D}(\varepsilon_{11},\varepsilon_{22}=0)-P_1^{2D}(\varepsilon_{11}=0,\varepsilon_{22}=0)=e_{11}^{2D}\varepsilon_{11}, \quad (2a)$$

$$P_2^{2D}(\varepsilon_{11}=0,\varepsilon_{22})-P_2^{2D}(\varepsilon_{11}=0,\varepsilon_{22}=0)=e_{22}^{2D}\varepsilon_{22}. \quad (2b)$$

respectively. To evaluate the planner elastic stiffness coefficients C_{11}^{2D},C_{22}^{2D} and C_{12}^{2D} of these two possible candidate piezoelectrics, we calculated the unit-cell energy U to a series of 2D strain states (ε_{11},ε_{22}) in a 11×11 grid. The results are shown in Fig. 5. Due to the mirror symmetry along the tube (y direction), we can obtain the elastic stiffness coefficients through fit the changes of unit-cell energy to the following equation:

$$\Delta U=\frac{1}{2}C_{11}^{2D}\varepsilon_{11}^2+\frac{1}{2}C_{22}^{2D}\varepsilon_{22}^2+C_{12}^{2D}\varepsilon_{11}\varepsilon_{22}.$$

where ΔU=[U($\varepsilon_{11},\varepsilon_{22}$) − $U(\varepsilon_{11}=0,\varepsilon_{22}=0)$]/$A_0$. A_0 is the equilibrium area of the corresponding system. According to the definitions of strain and stress, the relation between e_{ijk}^{2D}, d_{ijk}^{2D} and C_{ij}^{2D} can be build as

$$d_{11}^{2D}=\frac{e_{11}C_{22}-e_{12}C_{12}}{C_{11}C_{22}-C_{12}^2}, \quad d_{12}^{2D}=\frac{e_{12}C_{11}-e_{11}C_{12}}{C_{11}C_{22}-C_{12}^2}. \quad (3)$$

In our calculations, we chose the "relaxed-io" mode [12] to calculate the change of polarization contributed by both atoms relaxion and electrons rearrangement. Namely, all the atomic positions are fully relaxed under each strain before the polarization calculation. We firstly considered the single layered SnSe as reference system to check our calculation settings. In Table I, we show the piezoelectric coefficients e_{11}^{2D} and e_{12}^{2D} of SnSe calculated without van der Waals modification and its corresponding elastic stiffness coefficients C_{11}^{2D}, C_{22}^{2D} and C_{12}^{2D}. Based on these results, we calculated the coefficients d_{11}^{2D} and d_{12}^{2D} of SnSe to be 280.82 pm/V and −91.73 pm/V. These results are in good agreement with previous reports [5, 6], which indicate that our present calculation settings are reasonable. As shown in Table I, we can see that the results with van der Waals modification will be slightly overestimated in comparison with those without van der Waals modification.

The results of polarization changes for PNT(0,0.5) and PNT(30,0.5) are shown in Fig. 6 (a) and (b), respectively. According to the corresponding slope, the piezoelectric coefficients e_{11}^{2D} and e_{12}^{2D} can be calculated and are shown in Tab. I. Similarly, the calculated elastic stiffness coefficients C_{11}^{2D}, C_{22}^{2D} and C_{12}^{2D} for PNT(0,0.5) (PNT(30,0.5)) are also included in Tab. I. We can see that the piezoelectric coefficients e_{ij}^{2D} of PNT(0,0.5) and PNT(30,0.5) are very small in comparison with those of SnSe, but they are comparable to those of

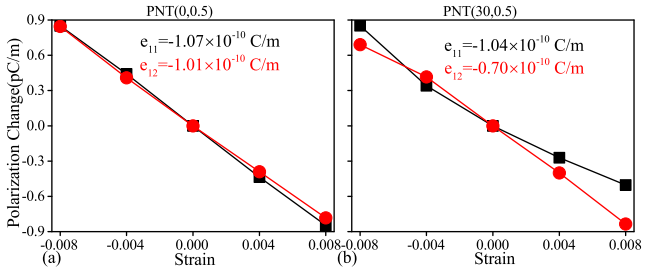

FIG. 6. Change of unit-cell polarization per area of PNT(0,0.5) (a) and PNT(30,0.5) (b) along the x direction after applying uniaxial strain ε_{11} (black solid square) and ε_{22} (red solid circle).

TABLE I. Calculated elastic coefficients C_{ij}^{2D} in units of N/m and piezoelectric coefficients e_{ij}^{2D} in 10^{-10} C/m and d_{ij}^{2D} in pm/V for SnSe, PNT(0,0.5) and PNT(30,0.5).

system	C_{11}^{2D}	C_{12}^{2D}	C_{22}^{2D}	e_{11}^{2D}	e_{12}^{2D}	d_{11}^{2D}	d_{12}^{2D}
SnSe[5]	19.88	18.57	44.49	34.9	10.8	250.57	-80.31
h-BN[12]	291	62	-	1.38	-	0.60	-
MoS_2[12]	130	32	-	3.64	-	3.73	-
SnSe	21.54	17.92	42.56	44.05	11.28	280.82	-91.73
SnSe-vdw	29.38	24.08	46.89	59.78	17.23	299.47	-117.05
PNT(0,0.5)	12.78	10.54	106.70	-1.07	-1.01	-8.26	-0.13
PNT(30,0.5)	13.80	9.90	105.21	-1.04	-0.70	-7.57	0.05
PNT(180,0.25)	14.17	7.48	102.73	-	-	-	-

h-BN and MoS_2 [12]. Especially, we notice that the elastic constants C_{ij}^{2D} of PNT(0,0.5) and PNT(30,0.5) are also very small in comparison with those of h-BN and MoS_2, which will significantly enhance the piezoelectric effects. From the calculated piezoelectric coefficients d_{11}^{2D} and d_{12}^{2D} for PNT(0,0.5) (as shown in Tab. I), we can see that the piezoelectric coefficients d_{11}^{2D} of PNT(0,0.5) and PNT(30,0.5) are larger than those of h-BN and MoS_2. Based on these results, we can predict that the x direction piezoelectric effects in PNT(0,0.5) and PNT(30,0.5) are more remarkable than those in h-BN and MoS_2.

FURTHER DISCUSSION

According to our knowledge, this is the first time we discovery piezoelectricity in a pure elementary material. These results indicate that elementary material can be ionic ones with polar dipole. We have carefully confirmed our results and got a good understanding. Such results are not strange things but understandable things by symmetry. The previous literatures about the ionic pure boron [62] phase and the metallic boron nitride [63, 64] phase enhance our confidence to believe our present results.

In fact, the intrinsic piezoelectricity in PNT(0,0.5) and PNT(30,0.5) as well as the absence of piezoelectricity in PNT(180,0.25) can be well understood by their structural symmetries, surface charge distributions (Fig. 7) and dipoles (Fig. 8), as well as the averaged electrostatic potentials (polarization field as indicated in Fig. 9. As shown in Fig. 7, the redistributed charge densities of PNT(0,0.5), PNT(30,0.5) and PNT(180, 0) are plotted to qualitatively study the charge transfer in these systems. We can see that in these phosphorene allotropes, the electrons transfer form the isolated atoms to the sp^3-orbits after bonding (See the partial P_8 molecule) to each other. Due to the equal electronegativity, there is no obvious electron transfer between P atoms, which makes the these phosphorene allotropes are covalent systems. However, the unequal sp^3-hybridizations of P atom makes the single PNT is a polar system (weak ionic like the high-pressure boron phase [62]). Further assembly PNTs to 2D array will enhance or weaken the polarization of the systems depending on the spacial orientations between PNTs.

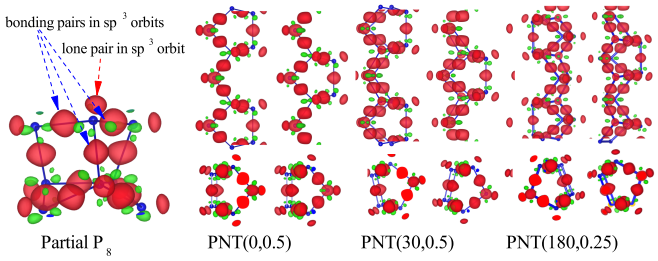

FIG. 7. Isosurface showings of the redistributed charge densities of PNT(0,0.5), PNT(30,0.5) and PNT(180, 0.25). An enlarged picture of the redistributed charge density of a partial P_8 molecule is also plotted to show the four unequal sp^3-hybridized orbits in these phosphorene allotropes.

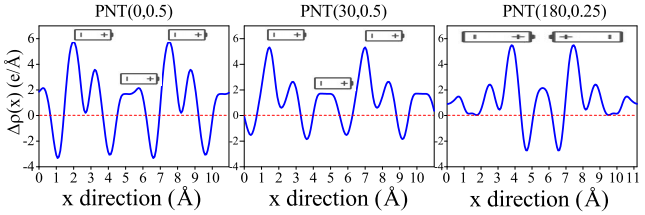

FIG. 8. The averaged redistributed charge densities along x-direction of PNT(0,0.5), PNT(30,0.5) and PNT(180, 0.25).

As shown in Fig. 8, the averages of the redistributed charge densities of PNT(0,0.5), PNT(30,0.5) and PNT(180, 0) are also shown for the purpose of indicating the dipole effects in these systems. We can see that the dipoles in PNT(0,0.5)

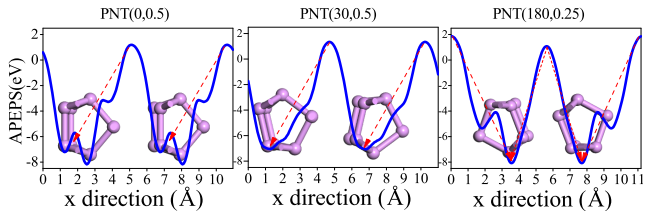

FIG. 9. The averaged electrostatic potentials along x-direction of PNT(0,0.5), PNT(30,0.5) and PNT(180, 0.25).

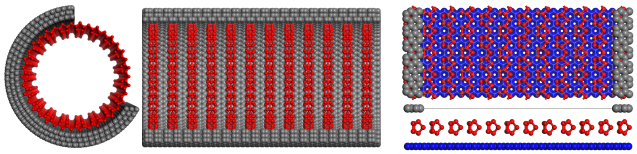

(a) PNT in multi-layered CNT (b) PNT array in graphene bi-layer

FIG. 10. Hypothetical models of PNT arrays synthesized within carbon nanotube nanoreactor (a) and graphene bilayer nanoreactor (b).

and PNT(30, 0.5) are additive enhancement, which indicate that both can be potential piezoelectric systems. However, the dipoles in PNT(180, 0) are subtractive due to the inversion center, which make the system non-piezoelectric. Consequently, the average planar electrostatic potentials (Fig. 9) of PNT(0,0.5), PNT(30,0.5) and PNT(180, 0) are also discussed here to show the polarization field in these systems. We can see that in both PNT(0,0.5) and PNT(30, 0.5), the polarization filed caused by the two single-PNTs have same polar direction, which make the system possess strong polarization filed in their inner body along the x-direction. However, the polarization field caused by the two single-PNTs in PNT(180, 0) have contrary direction and PNT(180,0) is consequently nonpolar. These results can help us to understand the piezoelectricity in PNT(30,0.5) and PNT(180, 0) well.

PNT(0,0.5) and PNT(30,0.5) possess remarkable stability and excellent piezoelectricity exceeding than h-BN and MoS_2 are highly expected to give rise wide interests in materials science, nano-electronics and condensed physics. They are highly expected to be synthesized in experiment due to their remarkable energetic stability. We noticed that the ring-shaped PNTs proposed by Liu[40] have been successfully synthesized by Zhang[41] in carbon nanotube nanoreactors (Fig. 10 (a)). We also find that the interlamination between graphene layers can be considered as an optional reactor to assembly these PNTs into 2D array as shown in Fig. 10 (b). We expect further experiments can be paid on assembly these PNTs into 2D arrays in the interlamination between graphene layers.

CONCLUSION

In summary, based on the previously proposed ultrathin metastable phosphorus nanotube, we predicted a new class of 2D van der Waals crystals for phosphorus through operations of translation and self-rotation. This new class of 2D phosphorene allotropes possess remarkable stabilities due to the strong inter-tube van der Waals interactions. They are of about 30-70 meV/atom lower in energy than the single um-PNT depending on the assembly. Our results show that most of these 2D van der Waals phosphorene allotropes are energetically more stable than the experimentally viable α-P and β-P. Three of them showing relatively higher probability to be synthesized in future deposition methods were also confirmed to be dynamically stable semiconductors with strain-tunable band gaps. Especially, two of them belonging to polar space groups were predicted to possess an impressive piezoelectricity higher than h-BN and MoS_2. Hence they have promising applications for nano-sized sensors, piezotronics, and energy harvesting in portable electronic nano-devices.

ACKNOWLEDGEMENT

This work is supported by the National Natural Science Foundation of China (Grant Nos. 11704319, 11647063, A040204, 11474244), the National Basic Research Program of China (2015CB921103), the Scientific Research Found of Hunan Provincial Education department (Nos. 14C1095, 17K086), the Natural Science Foundation of Hunan Province, China (Grant No. 2016JJ3118), the Program for Changjiang Scholars and Innovative Research Team in University (IRT13093), and the Furong Scholar Program of Hunan Provincial Government (RAR). UK research data statement: All data accompanying this publication are directly available within the publication.

* hechaoyu@xtu.edu.cn
† tang_chao@xtu.edu.cn
‡ r.roemer@warwick.ac.uk
§ jxzhong@xtu.edu.cn

[1] W. Wu, L. Wang, Y. Li, F. Zhang, L. Lin, S. Niu, D. Chenet, X. Zhang, Y. Hao, T. F. Heinz, , J. Hone and Z. Wang, Piezoelectricity of single-atomic-layer MoS_2 for energy conversion and piezotronics, Nature **514**, 470 (2014).

[2] H. Zhu, Y. Wang, J. Xiao, M. Liu, S. Xiong, Z. J. Wong, Z. Ye, Y. Ye, X. Yin and X. Zhang, Observation of piezoelectricity in free-standing monolayer MoS_2, Nat. Nanotechnol. **10**, 151 (2015).

[3] J. Qi, Y.-W. Lan, A. Z. Stieg, J.-H. Chen, Y.-L. Zhong, L.-J. Li, C.-D. Chen, Y. Zhang and K. L. Wang, Piezoelectric effect in chemical vapour deposition-grown atomic-monolayer triangular molybdenum disulfide piezotronics, Nature Communications **6**, 7430 (2015).

[4] M. Zelisko, Y. Hanlumyuang, S. Yang, Y. Liu, C. Lei, J. Li, P. M. Ajayan and P. Sharma, Anomalous piezoelectricity in two-dimensional graphene nitride nanosheets, Nature communications **5**, ncomms5284 (2014).

[5] L. C. Gomes, A. Carvalho and A. C. Neto, Enhanced piezoelectricity and modified dielectric screening of two-dimensional group-IV monochalcogenides, Phys. Rev. B **92**, 214103 (2015).

[6] R. Fei, W. Li, J. Li and L. Yang, Giant piezoelectricity of monolayer group IV monochalcogenides: SnSe, SnS, GeSe, and GeS, Appl. Phys. Lett. **107**, 173104 (2015).

[7] M. N. Blonsky, H. L. Zhuang, A. K. Singh and R. G. Hennig, Ab initio prediction of piezoelectricity in two-dimensional materials, ACS Nano **9**, 9885 (2015).

[8] K. H. Michel, D. Çakır, C. Sevik and F. M. Peeters, Piezoelectricity in two-dimensional materials: Comparative study between lattice dynamics and ab initio calculations, Physical Review B **95** (2017).

[9] M. M. Alyrk, Y. Aierken, D. Çakır, F. M. Peeters and C. Sevik, Promising Piezoelectric Performance of Single Layer

Transition-Metal Dichalcogenides and Dioxides, The Journal of Physical Chemistry C **119**, 23231 (2015).

[10] K. Kaasbjerg, K. S. Thygesen and A.-P. Jauho, Acoustic phonon limited mobility in two-dimensional semiconductors: Deformation potential and piezoelectric scattering in monolayer MoS2from first principles, Physical Review B **87** (2013).

[11] A. Thilagam, Ultrafast exciton relaxation in monolayer transition metal dichalcogenides, Journal of Applied Physics **119**, 164306 (2016).

[12] K.-A. N. Duerloo, M. T. Ong and E. J. Reed, Intrinsic piezoelectricity in two-dimensional materials, The Journal of Physical Chemistry Letters **3**, 2871 (2012).

[13] H. L. Zhuang, M. D. Johannes, M. N. Blonsky and R. G. Hennig, Computational prediction and characterization of single-layer CrS2, Applied Physics Letters **104**, 022116 (2014).

[14] R. Gao and Y. Gao, Piezoelectricity in two-dimensional group III-V buckled honeycomb monolayers, physica status solidi (RRL) - Rapid Research Letters **11**, 1600412 (2017).

[15] K. Michel and B. Verberck, Theory of elastic and piezoelectric effects in two-dimensional hexagonal boron nitride, Physical Review B **80**, 224301 (2009).

[16] H. Zheng, X. Li, N. Chen, S. Xie, W. Q. Tian, Y. Chen, H. Xia, S. Zhang and H.-B. Sun, Monolayer II-VI semiconductors: A first-principles prediction, Physical Review B **92**, 115307 (2015).

[17] P. Z. Hanakata, A. Carvalho, D. K. Campbell and H. S. Park, Polarization and valley switching in monolayer group-IV monochalcogenides, Physical Review B **94** (2016).

[18] H. Wang and X. Qian, Two-dimensional multiferroics in monolayer group IV monochalcogenides, 2D Materials **4**, 015042 (2017).

[19] T. Hu and J. Dong, Two new phases of monolayer group-IV monochalcogenides and their piezoelectric properties, Physical Chemistry Chemical Physics **18**, 32514 (2016).

[20] H. Tian, J. Tice, R. Fei, V. Tran, X. Yan, L. Yang and H. Wang, Low-symmetry two-dimensional materials for electronic and photonic applications, Nano Today **11**, 763 (2016).

[21] Y. Qin, X. Wang and Z. L. Wang, Microfibre–nanowire hybrid structure for energy scavenging, Nature **451**, 809 (2008).

[22] Z. L. Wang and J. Song, Piezoelectric nanogenerators based on zinc oxide nanowire arrays, Science **312**, 242 (2006).

[23] L. Li, Y. Yu, G. J. Ye, Q. Ge, X. Ou, H. Wu, D. Feng, X. H. Chen and Y. Zhang, Black phosphorus field-effect transistors, Nat. Nanotechnol. **9**, 372 (2014).

[24] H. Liu, A. T. Neal, Z. Zhu, Z. Luo, X. Xu, D. Tománek and D. Y. Peide, Phosphorene: an unexplored 2D semiconductor with a high hole mobility, ACS Nano (2014).

[25] J. Qiao, X. Kong, Z. Hu, F. Yang and W. Ji, High-mobility transport anisotropy and linear dichroism in few-layer black phosphorus, Nature communications **5** (2014).

[26] L. Liang, J. Wang, W. Lin, B. G. Sumpter, V. Meunier and M. Pan, Electronic bandgap and edge reconstruction in phosphorene materials, Nano Lett **14**, 6400 (2014).

[27] Z. Zhu and D. Tománek, Semiconducting layered blue phosphorus: a computational study, Phys. Rev. Lett. **112**, 176802 (2014).

[28] J. L. Zhang, S. Zhao, C. Han, Z. Wang, S. Zhong, S. Sun, R. Guo, X. Zhou, C. D. Gu, K. D. Yuan, , Z. Li and W. Chen, Epitaxial growth of single layer blue phosphorus: a new phase of two-dimensional phosphorus, Nano Lett. **16**, 4903 (2016).

[29] J. R. Brent, N. Savjani, E. A. Lewis, S. J. Haigh, D. J. Lewis and P. O'Brien, Production of few-layer phosphorene by liquid exfoliation of black phosphorus, Chem. Commun. **50**, 13338 (2014).

[30] J. B. Smith, D. Hagaman and H.-F. Ji, Growth of 2D black phosphorus film from chemical vapor deposition, Nanotechnology **27**, 215602 (2016).

[31] X. Li, B. Deng, X. Wang, S. Chen, M. Vaisman, S.-i. Karato, G. Pan, M. L. Lee, J. Cha, H. Wang and H. Wang, Synthesis of thin-film black phosphorus on a flexible substrate, 2D Mater. **2**, 031002 (2015).

[32] J. Guan, Z. Zhu and D. Tománek, High stability of faceted nanotubes and fullerenes of multiphase layered phosphorus: a computational study, Phys. Rev. Lett. **113**, 226801 (2014).

[33] J. Guan, Z. Zhu and D. Tománek, Tiling phosphorene, ACS Nano **8**, 12763 (2014).

[34] T. Zhao, C. He, S. Ma, K. Zhang, X. Peng, G. Xie and J. Zhong, A new phase of phosphorus: the missed tricycle type red phosphorene, J. Phys.: Condens. Matter **27**, 265301 (2015).

[35] M. Wu, H. Fu, L. Zhou, K. Yao and X. C. Zeng, Nine new phosphorene polymorphs with non-honeycomb structures: a much extended family, Nano Lett **15**, 3557 (2015).

[36] C. He, C. Zhang, C. Tang, T. Ouyang, J. Li and J. Zhong, Five low energy phosphorene allotropes constructed through gene segments recombination, Sci. Rep. **7** (2017).

[37] G. Schusteritsch, M. Uhrin and C. J. Pickard, Single-layered Hittorfs phosphorus: a wide-bandgap high mobility 2D material, Nano Letters **16**, 2975 (2016).

[38] Z. Zhuo, X. Wu and J. Yang, Two-Dimensional Phosphorus Porous Polymorphs with Tunable Band Gaps, J. Am. Chem. Soc **138**, 7091 (2016).

[39] M. Xu, C. He, C. Zhang, C. Tang and J. Zhong, First-principles prediction of a novel hexagonal phosphorene allotrope, physica status solidi (RRL)-Rapid Research Letters **10**, 563 (2016).

[40] D. Liu, J. Guan, J. Jiang and D. Tománek, Unusually stable helical coil allotrope of phosphorus, Nano Lett **16**, 7865 (2016).

[41] J. Zhang, D. Zhao, D. Xiao, C. Ma, H. Du, X. Li, L. Zhang, J. Huang, H. Huang, C. Jia, D. Tománek and C. Niu, Assembly of Ring-Shaped Phosphorus within Carbon Nanotube Nanoreactors, Angewandte Chemie **129**, 1876 (2017).

[42] G. C. Constantinescu and N. D. Hine, Multipurpose black-phosphorus/hBN heterostructures, Nano Lett **16**, 2586 (2016).

[43] J. Padilha, A. Fazzio and A. J. da Silva, van der Waals heterostructure of phosphorene and graphene: tuning the Schottky barrier and doping by electrostatic gating, Phys. Rev. Lett. **114**, 066803 (2015).

[44] Y. Cai, G. Zhang and Y.-W. Zhang, Electronic properties of phosphorene/graphene and phosphorene/hexagonal boron nitride heterostructures, The Journal of Physical Chemistry C **119**, 13929 (2015).

[45] C. Sevik, D. Cakır, O. Gulseren and F. M. Peeters, Peculiar Piezoelectric Properties of Soft Two-Dimensional Materials, The Journal of Physical Chemistry C **120**, 13948 (2016).

[46] J. P. Perdew, Density-functional approximation for the correlation energy of the inhomogeneous electron gas, Phys. Rev. B **33**, 8822 (1986).

[47] G. Kresse and J. Furthmüller, Efficient iterative schemes for ab initio total-energy calculations using a plane-wave basis set, Phys. Rev. B **54**, 11169 (1996).

[48] G. Kresse and J. Furthmüller, Efficiency of ab-initio total energy calculations for metals and semiconductors using a plane-wave basis set, Computational materials science **6**, 15 (1996).

[49] P. E. Blöchl, Projector augmented-wave method, Phys. Rev. B **50**, 17953 (1994).

[50] G. Kresse and D. Joubert, From ultrasoft pseudopotentials to the projector augmented-wave method, Phys. Rev. B **59**, 1758 (1999).

[51] J. Klimeš, D. R. Bowler and A. Michaelides, Chemical accuracy for the van der Waals density functional, J. Phys.: Condens. Matter **22**, 022201 (2009).

[52] J. Klimeš, D. R. Bowler and A. Michaelides, Van der Waals density functionals applied to solids, Phys. Rev. B **83**, 195131 (2011).

[53] S. Grimme, Semiempirical GGA-type density functional constructed with a long-range dispersion correction, Journal of Computational Chemistry **27**, 1787 (2006).

[54] T. Bučko, J. Hafner, S. Lebégue and J. G. Ángyán, Improved Description of the Structure of Molecular and Layered Crystals: Ab Initio DFT Calculations with van der Waals Corrections, The Journal of Physical Chemistry A **114**, 11814 (2010).

[55] K. Parlinski, Z. Li and Y. Kawazoe, First-principles determination of the soft mode in cubic ZrO 2, Phys. Rev. Lett. **78**, 4063 (1997).

[56] F. Bachhuber, J. von Appen, R. Dronskowski, P. Schmidt, T. Nilges, A. Pfitzner and R. Weihrich, The extended stability range of phosphorus allotropes, Angew. Chem. Int. Ed. **53**, 11629 (2014).

[57] M. Ruck, D. Hoppe, B. Wahl, P. Simon, Y. Wang and G. Seifert, Fibrous red phosphorus, Angew. Chem. Int. Ed. **44**, 7616 (2005).

[58] Y. Aierken, O. Leenaerts and F. M. Peeters, Defect-induced faceted blue phosphorene nanotubes, Phys. Rev. B **92**, 104104 (2015).

[59] D. Çakır, C. Sevik and F. M. Peeters, Significant effect of stacking on the electronic and optical properties of few-layer black phosphorus, Phys. Rev. B **92**, 165406 (2015).

[60] D. Çakır, H. Sahin and F. M. Peeters, Tuning of the electronic and optical properties of single-layer black phosphorus by strain, Phys. Rev. B **90**, 205421 (2014).

[61] J. F. Nye, Physical properties of crystals: their representation by tensors and matrices, Oxford university press (1985).

[62] A. R. Oganov, J. Chen, C. Gatti, Y. Ma, Y. Ma, C. W. Glass, Z. Liu, T. Yu, O. O. Kurakevych and V. L. Solozhenko, Ionic high-pressure form of elemental boron, Nature **457**, 863 (2009).

[63] J. Dai, X. Wu, J. Yang and X. C. Zeng, Unusual Metallic Microporous Boron Nitride Networks, The Journal of Physical Chemistry Letters **4**, 3484 (2013).

[64] S. Zhang, Q. Wang, Y. Kawazoe and P. Jena, Three-Dimensional Metallic Boron Nitride, Journal of the American Chemical Society **135**, 18216 (2013).